

Supplementary Information

High adsorption selectivity, capacity and rate of fructose by Metal–Organic Frameworks with abundant zirconium open metal sites

Hai-Long He^{a, d}, Zhongqi Liu^{a, d}, Fengqing Liu^e, Jie Chen^{a, d}, Pu Wang^{a, d}, Xianfeng Yi^e, Anmin Zheng^e, and Lei Wang^{a, b, c, d*}

^a School of Engineering, Westlake University, Hangzhou, Zhejiang 310024, China

^b Zhejiang Key Laboratory of Low-Carbon Intelligent Synthetic Biology, Westlake University, Hangzhou, Zhejiang 310030, China

^c Research Center for Industries of the Future, Westlake University, Hangzhou, Zhejiang 310030, China

^d Institute of Advanced Technology, Westlake Institute for Advanced Study, Hangzhou, Zhejiang 310024, China

^e State Key Laboratory of Magnetic Resonance and Atomic and Molecular Physics, National Center for Magnetic Resonance in Wuhan, Wuhan Institute of Physics and Mathematics, Innovation Academy for Precision Measurement Science and Technology, Chinese Academy of Sciences, Wuhan, Hubei 430071, China

Corresponding authors

*E-mail: wang_lei@westlake.edu.cn

Table of contents

1. Data statistics
2. Experimental procedures
 - 2.1 Breakthrough experiment setup
 - 2.2 Derivation of correction equations for equilibrium concentrations
 - 2.3 Schematic structure of low connectivity number MOF
 - 2.4 Adsorption isotherms of MOF-808 for monosaccharide
 - 2.5 Adsorption thermodynamics of MOF-808 for sugar
 - 2.6 Adsorption kinetics fitted by different models
 - 2.7 SEM image of UiO-66-X
 - 2.8 TGA for UiO-66-X defect concentration
 - 2.9 Processing of ^{31}P MAS NMR spectra
3. Reference

Supplementary Information

1. Data statistics

Table S1. Selectivity factor of ion-exchange resin (modified by Ca^{2+}) and MOF in the adsorption separation of fructose and glucose.

Adsorbent	Selectivity factor	Ref.
Dowex 50W-X8	2.67	[1]
Dowex Monosphere 99/Ca	2.20	[2]
Dowex 50WX 4-400	2.40	[3]
Amberlite CR 1320 CA	1.42	[4]
NU-1008	5.7	[5]
NU-906	13.7	[5]

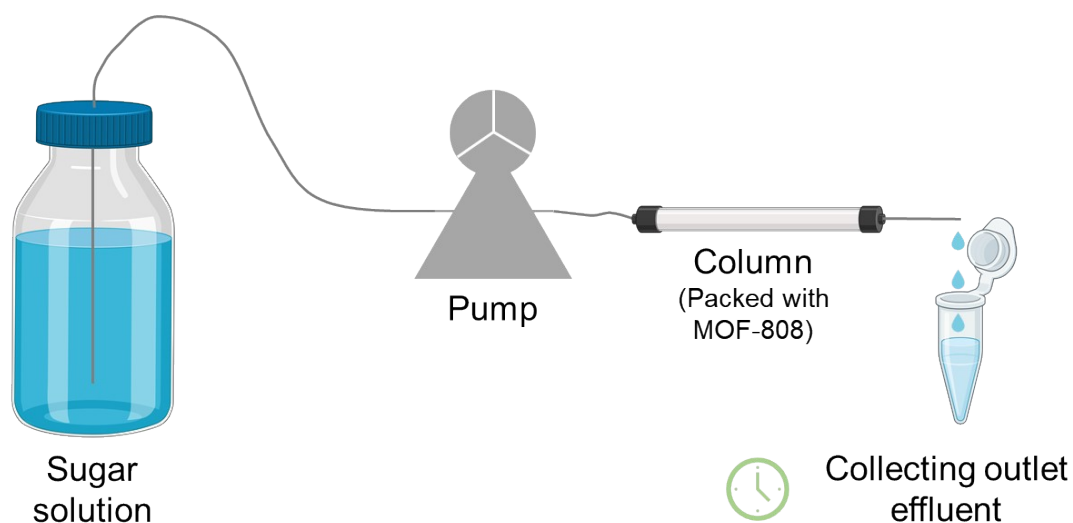
Table S2. Table of Zr_6 nodes connectivity number and pore size distribution (PSD) of MOF with their adsorption performance.

MOF	No. of connected	Pore size (nm)	Selectivity factor	Adsorption capacity (mg/g)	Kinetic constant (k_2) (g/(mg·h))	k_2q_c (h^{-1})	Ref.
UiO-66	12	1.96	3.51	63.2	0.113	6.98	[6]
NU-906	8	1	13.7	195	0.007	0.728	[5]
NU-1008	8	2.8	5.7	230	0.007	0.788	[5]
MOF-808	6	1.42	17.8	362	0.0603	18.9	This work

2. Experimental procedures

2.1 Breakthrough experiment setup

The breakthrough experimental setup is as follows:



Scheme S1. Setup of breakthrough experiment.

Supplementary Information

2.2 Derivation of correction equations for equilibrium concentrations

At initial time, in system

$$M_f + M_g + M_H = D$$

$$C_{0f} = M_f/D \quad C_{0g} = M_g/D \quad C_{0H} = M_H/D$$

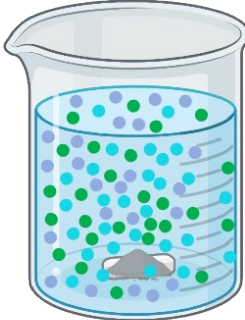
$$C_{0f} + C_{0g} + C_{0H} = 100 \text{ wt } \%$$

After equilibrium, fructose was adsorbed A_f , in system

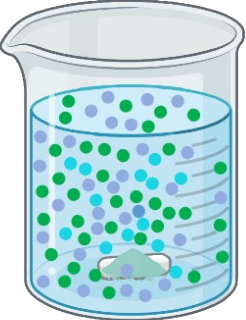
$$M'_f + M_g + M_H = D - A_f$$

$$C_{ef} = M'_f/(D-A_f) \quad C_{eg} = M_g/(D-A_f) \quad C_{eH} = M_H/(D-A_f)$$

$$C_{ef} + C_{eg} + C_{eH} = 100 \text{ wt } \%$$



Initial



Equilibrium

● Fructose (f) ● Glucose (g) ● H₂O (H)

Fru was obviously adsorbed, so $C_{0f} > C_{ef}$

Glu and H₂O were almost not adsorbed, and the mass was unchanged.

So, $C_{eg} = M_g/(D-A_f) > C_{0g} = M_g/D$

Even if glucose was adsorbed in small amounts, also $C_{eg} > C_{0g}$

Scheme S2. Schematic before and after competitive adsorption.

High fructose corn syrup contains three components: fructose, glucose and water (H₂O).

Initial: mass of glucose is M_g , mass of fructose is M_f , mass of H₂O is M_H .

So the initial concentration of glucose, fructose and H₂O is

$$C_{0g} = \frac{M_g}{(M_g + M_f + M_H)}$$

$$C_{0f} = \frac{M_f}{(M_g + M_f + M_H)}, \quad C_{0H} = \frac{M_H}{(M_g + M_f + M_H)}, \quad \text{and } C_{0g} + C_{0f} + C_{0H} = 100 \text{ wt } \%$$

Fructose was adsorbed A_f , and assuming that H₂O and glucose were not adsorbed.

Then, the equilibrium concentration of glucose, fructose and H₂O is

$$C_{eg} = \frac{M_g}{(M_g + M_f + M_H - A_f)}, \quad C_{ef} = \frac{M_f}{(M_g + M_f + M_H - A_f)},$$

$$C_{eH} = \frac{M_H}{(M_g + M_f + M_H - A_f)}, \quad C_{eg} + C_{ef} + C_{eH} = 100 \text{ wt } \%$$

Therefore, $\frac{C_{0H}}{C_{0g}} = \frac{M_H}{M_g} = \frac{C_{eH}}{C_{eg}}$, assuming the ratio is a , so

$$\frac{C_{0H}}{C_{0g}} = \frac{M_H}{M_g} = \frac{C_{eH}}{C_{eg}} = a \quad (\text{Eq. S1})$$

Because the mass concentration of the system before and after adsorption is 100 wt %, therefore, the reduced concentration of fructose ($C_{0f} - C_{ef}$) is equal to the sum of the increased concentrations of water and glucose. And assuming the increased

Supplementary Information

concentration of glucose is d .

$$\frac{C_{0H}}{C_{0g}} = a = \frac{aC_{0g}}{C_{0g}} = \frac{a(C_{0g} + d)}{C_{0g} + d} = \frac{aC_{0g} + ad}{C_{0g} + d} = \frac{C_{0H} + ad}{C_{0g} + d} = \frac{C_{eH}}{C_{eg}} \quad (\text{Eq. S2})$$

This means that when the increase in glucose concentration was d , the increase in H₂O concentration should be ad , so

$$ad + d = d(a + 1) = C_{0f} - C_{ef} \quad (\text{Eq. S3})$$

then,

$$d = \frac{(C_{0f} - C_{ef})}{a + 1} = \frac{(C_{0f} - C_{ef})}{\frac{C_{0H}}{C_{0g}} + 1} = \frac{(C_{0f} - C_{ef})}{\frac{(C_{0H} + C_{0g})}{C_{0g}}} = \frac{C_{0g}}{C_{0H} + C_{0g}} \cdot (C_{0f} - C_{ef})$$

(Eq. S4)

Therefore, the corrected equilibrium concentration of glucose (C_{eg}^*) should be

$$C_{eg}^* = C_{eg} - d = C_{eg} - \frac{C_{0g}}{C_{0H} + C_{0g}} \cdot (C_{0f} - C_{ef}) \quad (\text{Eq. S5})$$

Similarly, assuming that glucose adsorption leads to an increase in fructose concentration of k .

$$k = \frac{C_{0f}}{(C_{0H} + C_{0f})} \cdot (C_{0g} - C_{eg}^*) \quad (\text{Eq. S6})$$

So, the corrected equilibrium concentration of fructose (C_{ef}^*) should be

$$C_{ef}^* = C_{ef} - k = C_{ef} - \frac{C_{0f}}{C_{0H} + C_{0f}} \cdot (C_{0g} - C_{eg}^*) \quad (\text{Eq. S7})$$

More accurate equilibrium concentrations can be obtained by using a self-written code to perform several iterations of the above process on the values of k and d until convergence (change less than 10^{-6} mg/g).

The formula for calculating adsorption capacity is:

$$Q = (C_0 - C_e)M/m \quad (\text{Eq. S8})$$

When using the corrected equilibrium concentration, the equation should be

$$Q_g = (C_{0g} - C_{eg}^*)M/m \quad (\text{Eq. S9})$$

$$Q_f = (C_{0f} - C_{ef}^*)M/m \quad (\text{Eq. S10})$$

2.3 Schematic structure of low connectivity number MOF

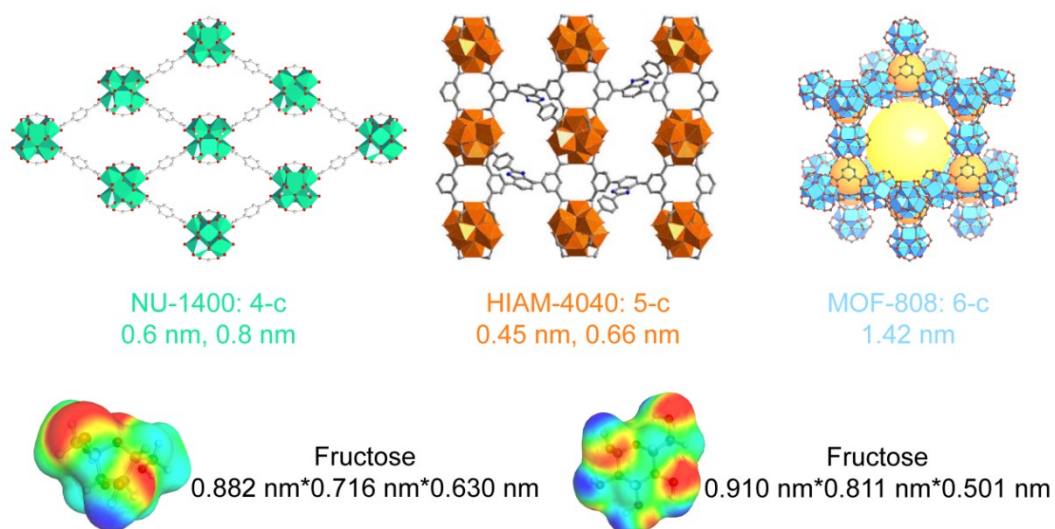


Figure S1. Schematic structure of low connectivity number MOF and structure of glucose and fructose. Adapted from reference [7-9].

2.4 Adsorption isotherms of MOF-808 for monosaccharide

Supplementary Information

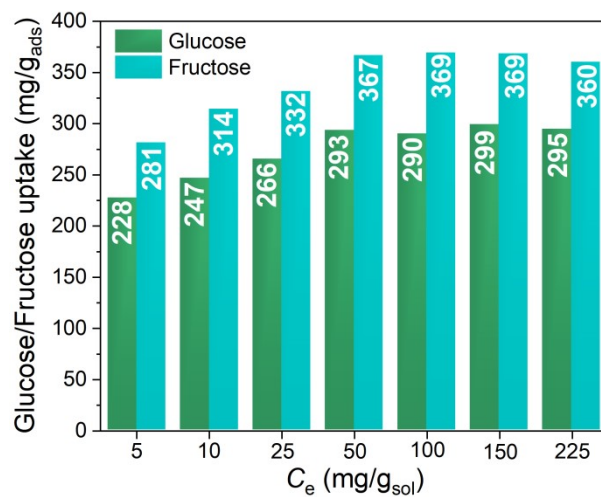


Figure S2. **Isothermal adsorption of monosaccharides.** The adsorption isotherms showed that the MOF-808 adsorption reached saturation at a sugar concentration of 50 mg/g_{sol}.

2.5 Adsorption thermodynamics of MOF-808 for sugar

Supplementary Information

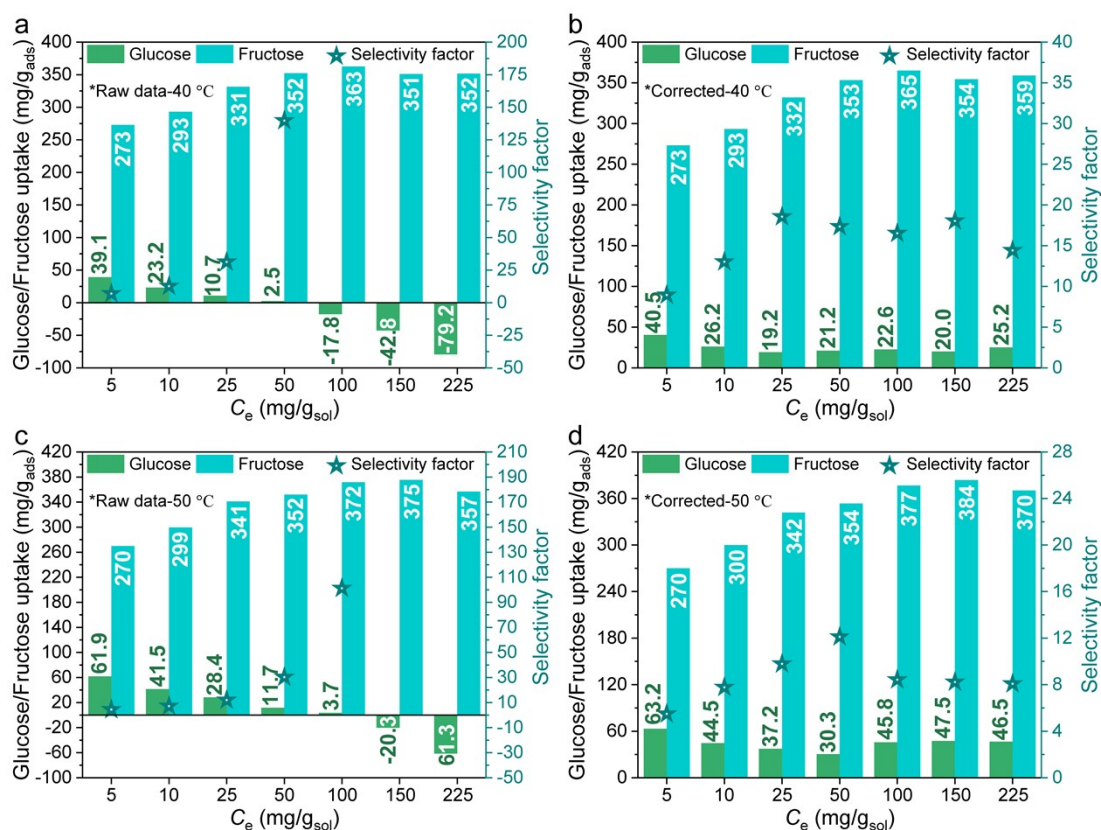


Figure S3. Competitive adsorption isotherms for fructose and glucose by MOF-808 at 40 °C (a, b) and 50 °C (c, d). a and c, The measured raw equilibrium concentrations were used to calculate the adsorption capacity and selectivity factor of MOF-808 for fructose and glucose. b and d, The adsorption capacity and selectivity factor were calculated utilizing the corrected equilibrium concentrations. The selectivity factor for the competitive adsorption at 50 °C was maintained above 8.0.

To explain the results of the competitive adsorption of glucose and fructose in MOF-808 at different temperatures, we determined the adsorption of single-component of glucose and fructose at different temperatures, from which we derived the thermodynamic parameters of their adsorption processes. The sugar concentration range selected here is the concentration when they are close to adsorption saturation. And the thermodynamic parameters of adsorption were determined using the following equations^[10].

$$\ln K_d = \frac{\Delta S^0}{R} - \frac{\Delta H^0}{RT} \quad (\text{Eq. S11})$$

where ΔS^0 is entropy change (J/(mol·K)), ΔH^0 is enthalpy change (J/mol), R is the universal gas constant (8.314 J/(mol·K)), T is the thermodynamic temperature (K), K_d is the distribution coefficient which can be calculated as:

Supplementary Information

$$K_d = \frac{C_{Ae}}{C_e} \quad (\text{Eq. S12})$$

where C_{Ae} (mg/g) is the adsorbed mass concentration at equilibrium (using the mass of adsorbed sugar divided by the sum of the masses of the sugar and adsorbent), C_e (mg/g) is the equilibrium mass concentration. In this study, the sugar concentration was selected to be 50 mg/g to calculate K_d , when adsorption is close to saturation.

And Gibbs free energy change (ΔG^0 , J/mol) can be calculated using the following equation:

$$\Delta G^0 = -RT \ln K_d \quad (\text{Eq. S13})$$

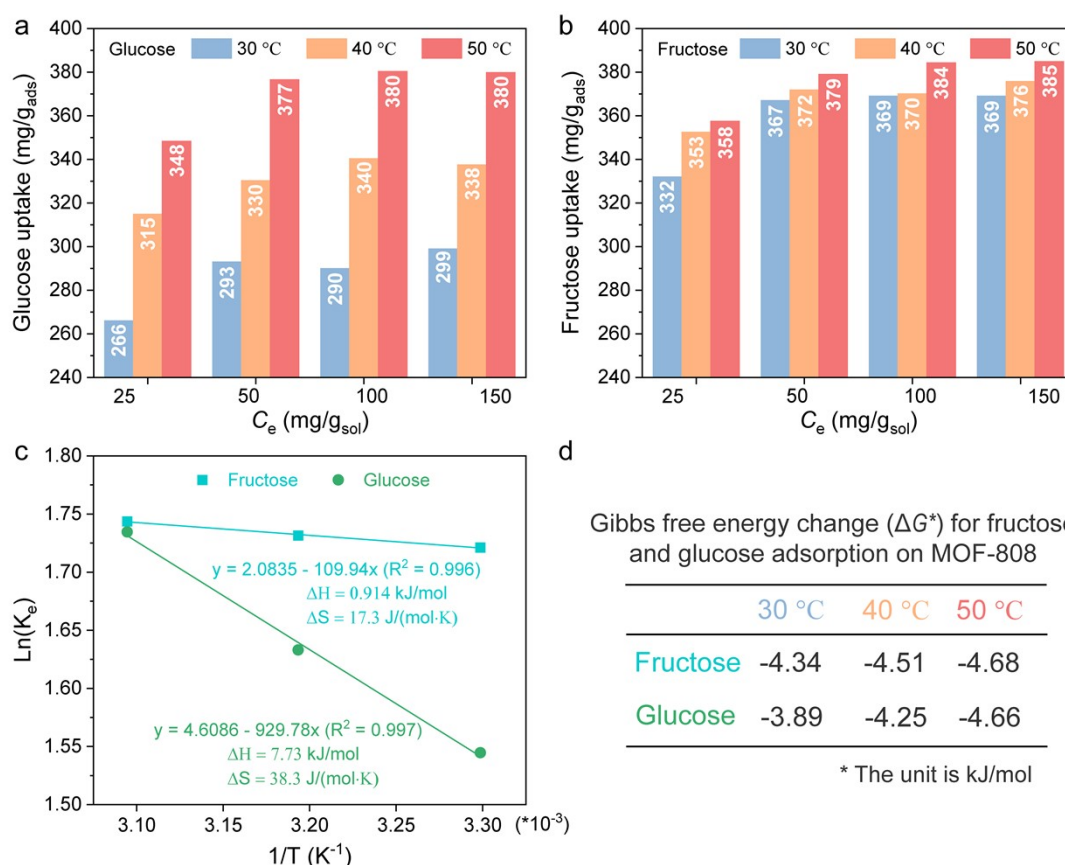


Figure S4. **Characterization of adsorption thermodynamics.** Adsorption isotherms for glucose (a) and fructose (b) at different temperatures; adsorption thermodynamic parameters derived from adsorption isotherm: enthalpy change and entropy change (c), and Gibbs free energy change (d).

2.6 Adsorption kinetics fitted by different models

The adsorption process consists of external diffusion (liquid film diffusion), intraparticle diffusion, and adsorption of the adsorbate onto the adsorption site (Scheme S3). In this study, four kinetic models were selected to fit the kinetic data, covering the three stages of the adsorption process described above.

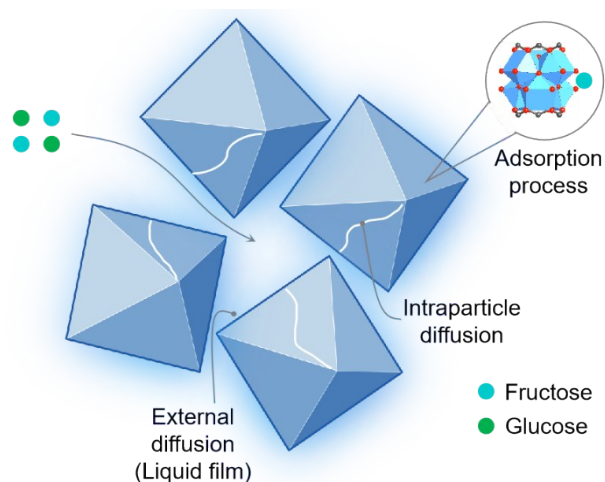
The Boyd model describes whether the diffusion process is controlled by external liquid film diffusion or intraparticle diffusion at the final stage, when the Bt vs. t linear curve passes through the origin (0, 0), indicating that diffusion is controlled by intraparticle diffusion, whereas when it does not pass through the origin, it is controlled by external liquid film diffusion.

The intraparticle diffusion model reflects whether the rate-limiting step in the adsorption process is an intraparticle diffusion process via the linear correlation between q_t and $t^{1/2}$.

The pseudo-first-order (PFO) model reflects whether the rate-limiting step in the adsorption process is a diffusion process, which includes both external liquid film diffusion and intraparticle diffusion, according to the linear correlation between $\ln(1 - q_t/q_e)$ and t .

The pseudo-second-order (PSO) model reflects whether the rate-limiting step in the adsorption process is the adsorption of the adsorbate onto the active site, namely, the chemisorption process, on the basis of the linear correlation between t/q_t and t .

Supplementary Information



Scheme S3. Schematic diagram of sugar diffusion and adsorption process.

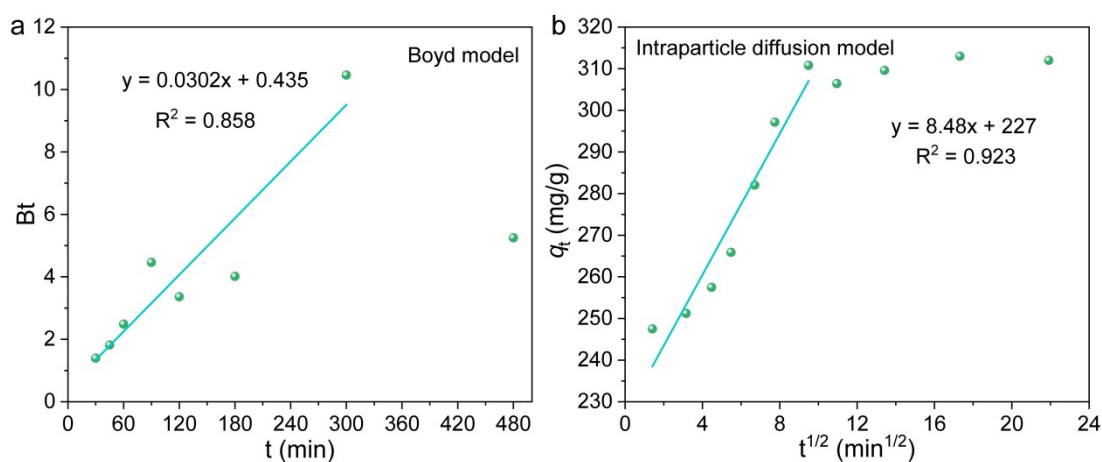


Figure S5. Adsorption kinetics fitted by different models: Boyd model ($30 \text{ min} \leq x \leq 300 \text{ min}$) (a) and Intraparticle diffusion model ($x < 10$) (b).

2.7 SEM image of UiO-66-X

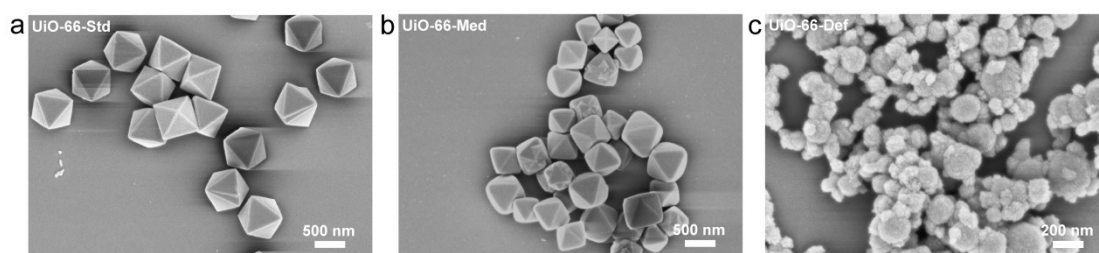


Figure S6. SEM image of UiO-66-Std (a), UiO-66-Med (b), UiO-66-Def (c).

2.8 TGA for UiO-66-X defect concentration

The change of Zr content in the UiO-66-X was characterized by the strategy of full oxidation to ZrO_2 at high temperatures in air, which responded to the change of defect concentration in the samples. And the defect concentration was obtained by the

Supplementary Information

following equation^[11]:

$$C_d = \frac{(\textit{theoretical mass loss}) - (\textit{experimental mass loss})}{\textit{theoretical mass loss}} \times 100\%$$

where the *theoretical mass loss* is calculated to be 0.444 (44.4%) by the chemical formula of UiO-66 ($\text{Zr}_6\text{O}_8\text{H}_4(\text{C}_8\text{H}_4\text{O}_4)_6$), the *experimental mass loss* is obtained by subtracting the mass after 1 hour of constant temperature at 900 °C from the mass at 380 °C (plateau) and dividing by the mass at 380 °C.

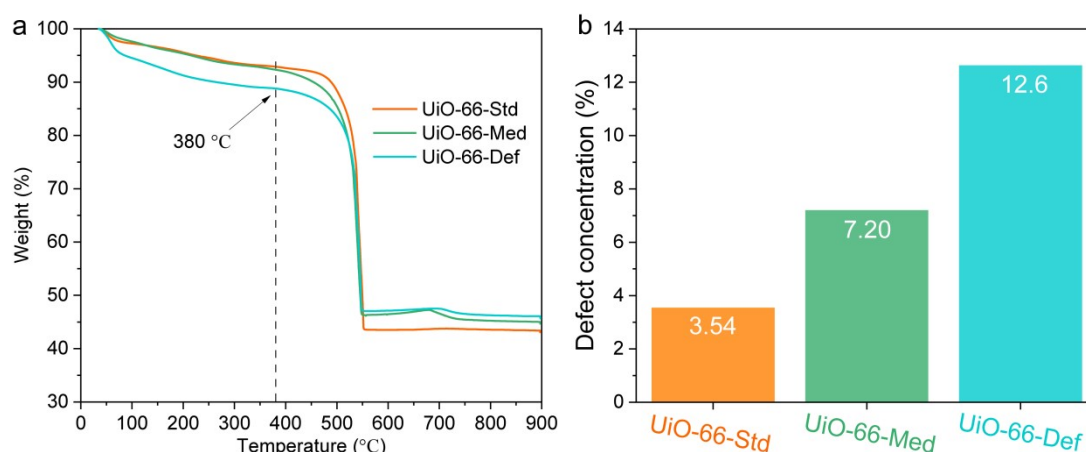


Figure S7. TGA characterized for defect concentration of UiO-66-X. **a**, The TGA curves indicate that the plateau before the mass loss was at about 380 °C; **b**, defect concentration values calculated from TGA curves.

2.9 Processing and normalization of ³¹P MAS NMR spectra

In order to visualize the NMR peak intensities to represent the information about the amount of Lewis acidic zirconium site per unit mass, we normalized the raw peak intensities of raw spectra based on the mass of each sample and obtained the following results:

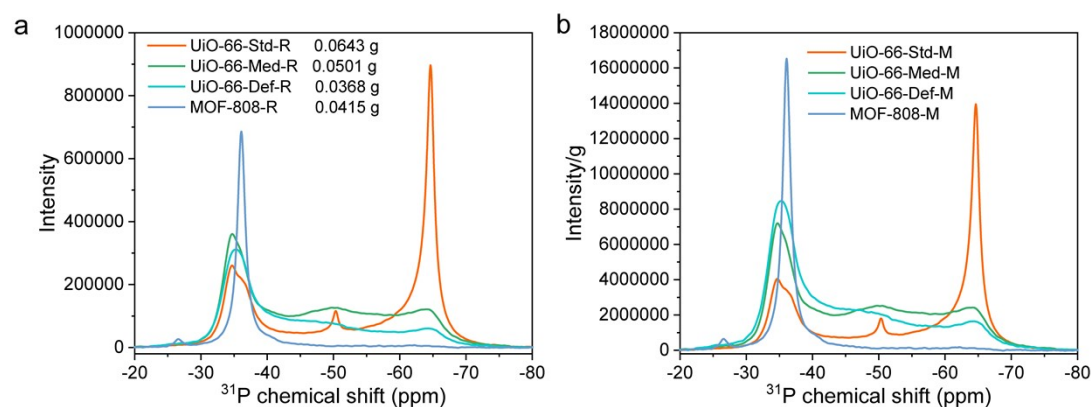


Figure S8. ³¹P MAS NMR spectra of TMP adsorbed on UiO-66-X and MOF-808 from raw data (**a**) and processed data based on sample mass (**b**).

3. Reference

- [1]. Y. S. Ghim and H. N. Chang, *Industrial & Engineering Chemistry Fundamentals*, 1982, 21, 369-374.
- [2]. M. Saska, S. J. Clarke, M. D. Wu and K. Iqbal, *Journal of Chromatography A*, 1992, 590, 147-151.
- [3]. J. A. Vente, H. Bosch, A. B. De Haan and P. J. T. Bussmann, *Chemical Engineering Communications*, 2005, 192, 23-33.
- [4]. M. Gramblicka and M. Polakovic, *J Chem Eng Data*, 2007, 52, 345-350.
- [5]. T. Xin, M. Chen, Z. Liu, R. Luo, Q. Xing, P. Bai, X. Guo and J. Lyu, *Separation and Purification Technology*, 2023, 319, 124038.
- [6]. Z. Zeng, J. Lyu, P. Bai and X. Guo, *Industrial & Engineering Chemistry Research*, 2018, 57, 9200-9209.
- [7]. Y. Zhang, X. Zhang, J. Lyu, K.-i. Otake, X. Wang, L. R. Redfern, C. D. Malliakas, Z. Li, T. Islamoglu, B. Wang and O. K. Farha, *Journal of the American Chemical Society*, 2018, 140, 11179-11183.
- [8]. H. Lyu, O. I. Chen, N. Hanikel, M. I. Hossain, R. W. Flaig, X. Pei, A. Amin, M. D. Doherty, R. K. Impastato, T. G. Glover, D. R. Moore and O. M. Yaghi, *Journal of the American Chemical Society*, 2022, 144, 2387-2396.
- [9]. T. Peng, C.-Q. Han, H.-L. Xia, K. Zhou, J. Zhang, J. Si, L. Wang, J. Miao, F.-A. Guo, H. Wang, L.-L. Qu, G. Xu, J. Li and X.-Y. Liu, *Chemical Science*, 2024, 15, 3174-3181.
- [10]. I. A. Tan, A. L. Ahmad and B. H. Hameed, *Journal of hazardous materials*, 2008, 154, 337-346.
- [11]. J. Duncan, D. Sengupta, S. Bose, K. O. Kirlikovali and O. K. Farha, *Sustainable Chemistry for the Environment*, 2023, 3, 100032.